STELLAR EVOLUTION. V. THE EVOLUTION OF A 15 $M_\odot$ STAR FROM THE MAIN SEQUENCE THROUGH CORE HELIUM BURNING*

Icko Iben, Jr.†
California Institute of Technology, Pasadena, and
Massachusetts Institute of Technology, Cambridge
Received July 12, 1965

ABSTRACT

The evolution of a 15 $M_\odot$ star of population I composition is described and compared with the evolution of less massive stars presented in earlier papers of this series and with the evolution of a 15.6 $M_\odot$ star calculated by Hayashi and his collaborators. During the core hydrogen-burning phase, the evolution of the 15 $M_\odot$ star is qualitatively almost identical with the evolution of the lighter stars. In the 15 $M_\odot$ star, during the phases of over-all contraction and hydrogen-shell development, matter becomes unstable against convection in a large region extending outward from the developing shell. The redistribution of composition variables in this region has an effect on the surface abundances when the star reaches the red-giant tip. Core helium burning in the 15 $M_\odot$ star occurs at much higher surface temperatures than is the case with less massive stars and requires a significantly longer time interval than that found for the 15.6 $M_\odot$ star. Contrary to the results of Hayashi and Cameron, the surface temperature of the 15 $M_\odot$ star decreases throughout the core helium-burning phase. Passage across the observational Cepheid strip and motion along the red-giant branch do not occur until near the end of the core helium-burning phase of the 15 $M_\odot$ star.

I. PRELIMINARY REMARKS

All constitutive relations and methods of solution used in the calculation of 15 $M_\odot$ evolution are identical with those described in Papers I–IV of this series (Iben 1965*a*, *b*; 1966*a*, *b*). Notation and symbols employed in the present paper are also the same as in Papers I–IV.

The pre–main-sequence evolution of the 15 $M_\odot$ star is discussed in Paper I. The description in the present work of evolution from the main sequence to the core helium-exhaustion phase is based on 500 models, each containing up to 320 mass shells. These numbers are governed by the necessity of meeting restrictions on time intervals between successive models and restrictions on mass shell sizes as described in Appendix A of Paper I.

II. PATHS IN THE HERTZSPRUNG-RUSSELL DIAGRAM AND COMPARATIVE LIFETIMES

The solid curve joining circled points in Figure 1 represents the evolutionary path of the 15 $M_\odot$ star (initial composition $X_H = 0.708$, $Z = 0.02$) in the Hertzsprung-Russell diagram when the center of mass cross-section for the $C^{12}(\alpha,\gamma)O^{16}$ reaction is chosen to be the same as in Paper II ($\sigma_{412} = \sigma^0_{412}$). When the $C^{12}(\alpha,\gamma)O^{16}$ cross-section is reduced by a factor of 10 ($\sigma_{412} = \sigma^0_{412}/10$), the path followed by the 15 $M_\odot$ model star is defined by the dashed curve. The solid line joining the boxed points represents the evolutionary track of the 15.6 $M_\odot$ model star (initial composition $X_H = 0.90$, $Z = 0.02$) computed by Sakashita, Ono, and Hayashi (1959) and by Hayashi and Cameron (1962*a*). Times to reach labeled points in Figure 1 are given in Table 1 in units of 10^7 yr.

Another comparison between the 15 $M_\odot$ star (with $\sigma_{412} = \sigma^0_{412}$) and the 15.6 $M_\odot$ star is made in Table 2, where absolute and relative time intervals associated with four evolutionary phases are given. The larger main-sequence lifetime and the lower luminosities

* Supported in part by the Office of Naval Research (Nonr-220(47)) and the National Aeronautics and Space Administration (NGR-05-002-028 and NSG-496).

†Now at Massachusetts Institute of Technology.

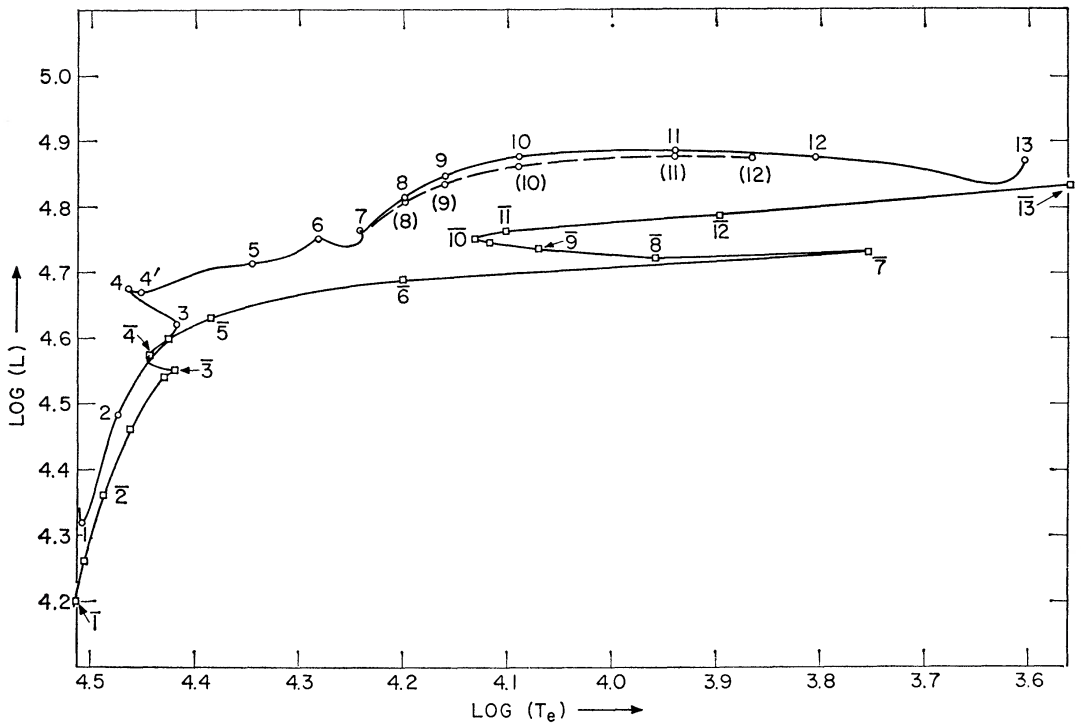

FIG. 1.—Paths in the theoretical Hertzsprung-Russell diagram for 15 $M_\odot$ and 15.6 $M_\odot$ stars of population I composition. The solid curve joining circled points defines the path of a 15 $M_\odot$ star (X_H = 0.708, Z = 0.02) when the larger (σ°_{412}) of two choices for the $C^{12}(\alpha,\gamma)O^{16}$ cross-section is used. The dashed curve defines the path of the 15 $M_\odot$ star (X_H = 0.708, Z = 0.02) when the smaller ($\sigma^\circ_{412}/10$) cross-section is used. The solid curve joining boxed points gives the path of a 15.6 $M_\odot$ star (X_H = 0.90, Z = 0.02) computed by Sakashita, Ono, and Hayashi (1959) and by Hayashi and Cameron (1962). Luminosity, L, is in units of $L_\odot = 3.86 \times 10^{33}$ ergs/sec and surface temperature, T_e, is in units of degrees Kelvin.

TABLE 1

EVOLUTIONARY LIFETIMES (10^7 YR)

Point	Time	Point	Time	Point	Time	Point	Time
1.....	0.0138224	8.....	1.113604	(10).....	1.172234	$\bar{6}$.....	1.88737
2.....	0.663253	9.....	1.154207	(11).....	1.196159	$\bar{7}$.....	1.88962
3.....	1.024045	10.....	1.192760	(12).....	1.198475	$\bar{8}$.....	1.88962+
4.....	1.046745	11.....	1.208043	$\bar{1}$.....	0.0	$\bar{9}$.....	1.92166
4′.....	1.047159	12.....	1.210199	$\bar{2}$.....	0.91	$\bar{10}$.....	1.97129
5.....	1.048983	13.....	1.211368	$\bar{3}$.....	1.87	$\bar{11}$.....	1.99117
6.....	1.050644	(8).....	1.106956	$\bar{4}$.....	1.88363	$\bar{12}$.....	2.00302
7.....	1.054302	(9).....	1.138944	$\bar{5}$.....	1.88460	$\bar{13}$.....	2.00505

TABLE 2

COMPARATIVE LIFETIMES (10^6 YR)

PHASE	15 $M_\odot$ ($\sigma_{412}=\sigma^0_{412}$)			15.6 $M_\odot$		
	Points	Δt	$(100\Delta t/t_{total})$	Points	Δt	$(100\Delta t/t_{total})$
Main sequence.....	1–3	10.24	84.53	$\bar{1}$–$\bar{3}$	18.7	93.26
Gravitational contraction...	3–4	0.2270	1.874	$\bar{3}$–$\bar{4}$	0.1363	0.68
Hydrogen-shell source.....	4′–7	0.07557	0.624	$\bar{4}$–$\bar{7}$	0.0599	0.30
Helium-burning core.....	7–13	1.571	12.97	$\bar{7}$–$\bar{13}$	1.1543	5.77
Total.....	1–13	12.1137	100.0	$\bar{1}$–$\bar{13}$	20.0505	100.0

during the core hydrogen-burning stage found by Sakashita *et al.* may be attributed to the choice of a larger initial hydrogen content. The larger time interval found here for the gravitational contraction phase may be ascribed in part to the fact that the transfer of energy to and from the gravitational field is computed at all points in the star, not just in the stellar core, as in the models constructed by Hayashi and Cameron. The inclusion of the $N^{14}(\alpha,\gamma)F^{18}(\beta^+\nu)O^{18}$ reactions in the present work accounts, in part, for the larger time spent by the 15 $M\odot$ star between the formation of the hydrogen-burning shell and the onset of the triple-α process in the stellar core. The difference in core helium-burning lifetimes between the 15 $M\odot$ and 15.6 $M\odot$ model stars cannot be due primarily to a difference in the choice of helium-burning rates, since a reduction by a factor of 10 in the $C^{12}(\alpha,\gamma)O^{16}$ cross-section reduces the helium-burning lifetime only from 1.571×10^6 yr ($\sigma_{412} = \sigma^0{}_{412}$) to 1.442×10^6 yr ($\sigma_{412} = \sigma^0{}_{412}/10$). The discrepancy may be due in part to a difference in the distribution of hydrogen within the stellar interior in the two cases.

The differences in the evolutionary paths in the H-R diagram following the exhaustion of central hydrogen (after points 4′ and $\bar{4}$ in Fig. 1) may be partially due to the fact that Hayashi and Cameron have chosen much larger time intervals. The evolution represented by the path between points 3 and $\bar{3}$ in Figure 1 has required the construction of over 400 models; evolution between points $\bar{3}$ and $\bar{13}$ has involved the construction of approximately twenty models.

III. FROM THE MAIN SEQUENCE TO THE ONSET OF THE TRIPLE-α PROCESS

The discussion in this section and in the following section concerns the case $\sigma_{412} = \sigma^0{}_{412}$. A discussion of the $\sigma_{412} = (\sigma^0{}_{412}/10)$ case is deferred until § V.

The variation with time of pertinent observable and interior characteristics, when $\sigma_{412} = \sigma^0{}_{412}$, is given in Figures 2–4. The behavior of the 15 $M\odot$ star during the core hydrogen-burning stage is qualitatively almost identical with the behavior of the 3 $M\odot$, 5 $M\odot$, and 9 $M\odot$ stars treated in the earlier papers of this series.

The only significant difference is the occurrence, in the 15 $M\odot$ star, of two convective layers just beyond the convective core. These layers are defined by the cross-hatched regions labeled M_{l1} and M_{l2} in Figure 2. In previous work on massive stars (e.g., Schwarzschild and Härm 1958; Sakashita and Hayashi 1961; Stothers 1963), these regions have been treated as semiconvective. Since the physical basis for the concept of semiconvection is not theoretically well established, it is felt that adherence in the present work to the simple treatment of convection is justified. During the main-sequence phase, the redistribution of hydrogen and helium in the convective layers beyond the convective core is inconsequential and has little effect on the evolutionary behavior of the star.

It is worthwhile to point out that, in spite of the high central temperatures in the 15 $M\odot$ star (see T_c versus t in Fig. 3), O^{16} in the convective core is not converted rapidly into N^{14} during the core hydrogen-burning phase (see X_{16} versus t in Fig. 2). In fact, O^{16} never does reach equilibrium with respect to N^{14} and the full CNO cycle does not operate during core hydrogen burning. This is due to the large size of the convective core (see M_{cc} in Fig. 2), which contains over one-third of the stellar mass near the main sequence. As a consequence of the large core, the average temperature sampled by a reacting particle is much lower than the central temperature.

Toward the end of the gravitational contraction phase (points 3–4 in Fig. 1), the relative decrease in the nuclear-energy production rate is considerably larger in the 15 $M\odot$ star than in any of the lighter stars studied previously (compare the curve log (L_n) versus t in Fig. 4 with the same curve for the 9 $M\odot$ star in Fig. 7 of Paper IV). This is a consequence of the much larger mass fraction over which hydrogen has been depleted during early evolution from the main sequence. In the 15 $M\odot$ star, the mass fraction in the convective core drops slowly from $M_{cc} \sim 0.394$ near the main sequence, to $M_{cc} \sim 0.183$ at $t = 1.0443 \times 10^7$ yr. Thereafter, due to the decrease in core nuclear-

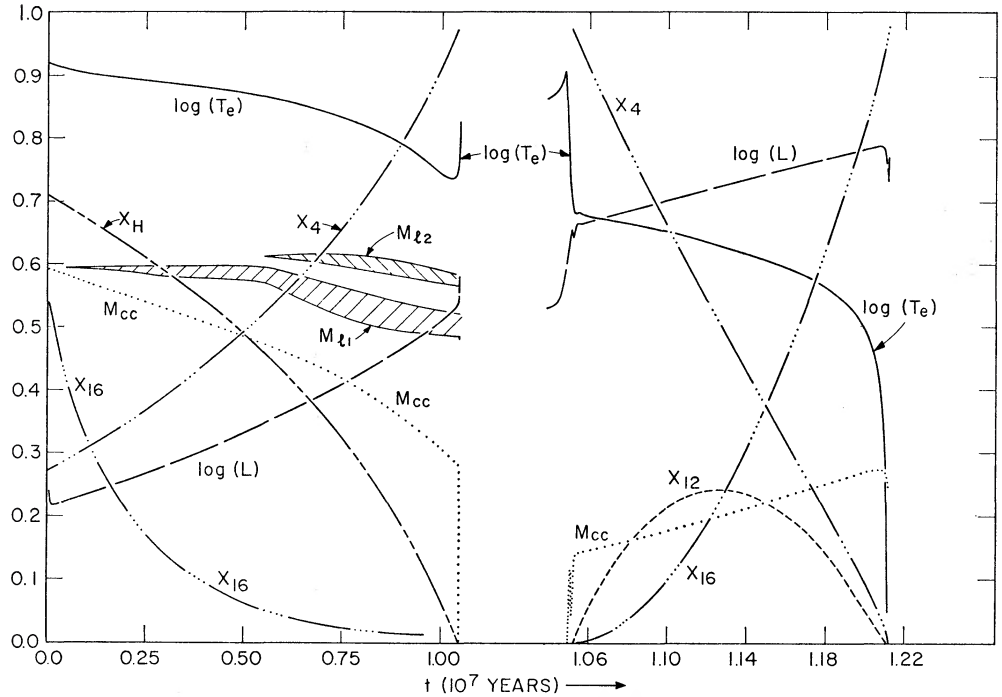

FIG. 2.—The variation with time t (units of 10^7 yr.) of luminosity (L), surface temperature (T_e), mass fraction in the convective core (M_{cc}), mass fractions in two convective layers (M_{l1} and M_{l2}), and central abundance by mass of $H^1(X_H)$, $He^4(X_4)$, $C^{12}(X_{12})$, and $O^{16}(X_{16})$. The unit of luminosity is $L_\odot = 3.86 \times 10^{33}$ ergs/sec and the unit of surface temperature is degrees Kelvin. To the left of the break in t, vertical scale limits correspond to $4.1 \leq \log (L) \leq 5.1$, $4.05 \leq \log (T_e) \leq 4.55$, $0.0 \leq M_{cc}, M_{l1}, M_{l2} \leq (\frac{2}{3})$ $0.0 \leq X_{16} \leq 0.02$, and $0.0 \leq X_H, X_4 \leq 1.0$. To the right of the break in t, scale limits correspond to $4.1 \leq \log (L) \leq 5.1$, $3.56 \leq \log (T_e) \leq 4.56$, $0.0 \leq M_{cc} \leq (\frac{2}{3})$, and $0.0 \leq X_4, X_{12}, X_{16} \leq 1.0$.

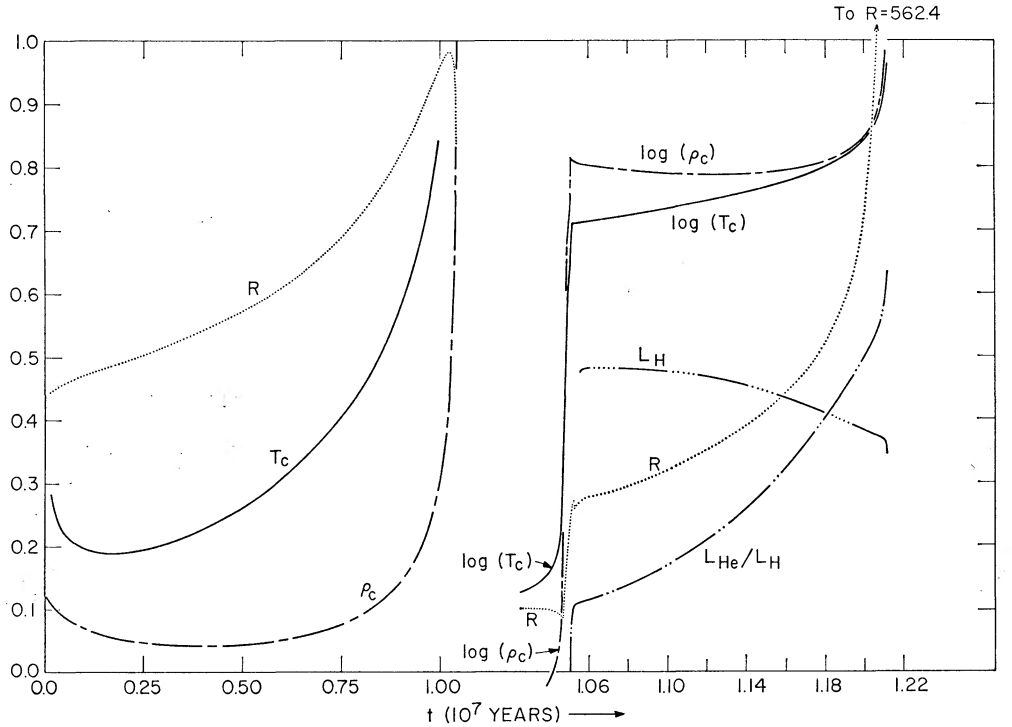

FIG. 3.—The variation with time t (units of 10^7 yr.) of radius (R), central density (ρ_c), central temperature (T_c), the rate of nuclear-energy production in the hydrogen-burning shell (L_H), and the rate of energy production by helium burning relative to the rate of energy production by hydrogen burning (L_{He}/L_H). Units are $R_\odot = 6.96 \times 10^{10}$ cm for radius, $10^{6\circ}$ K for temperature, gm/cm^{-3} for density, and $L_\odot = 3.86 \times 10^{33}$ ergs/sec for L_H. To the left of the break in t, scale limits correspond to $0.2 \leq R \leq 10.2$, $5 \leq \rho_c \leq 15$, and $31.6 \leq T_c \leq 41.6$. To the right of the break in t, $0 \leq R \leq 100$, $1.1 \leq \log (\rho_c) \leq 3.6$, $1.5 \leq \log (T_c) \leq 2.5$, $0 \leq L_H \leq 10^5$, and $0 \leq L_{He}/L_H \leq 2.0$.

energy production, the rate at which the core shrinks in mass fraction begins to accelerate. In the 9 $M\odot$ star, the convective core shrinks in mass fraction from $M_{cc} \sim 0.30$ to $M_{cc} \sim 0.12$, before decreasing rapidly at the end of the gravitational-contraction phase.

Between $t = 1.04462 \times 10^7$ yr and $t = 1.04666 \times 10^7$ yr, the rate of nuclear-energy production in the 15 $M\odot$ star drops from $L_n \sim 42660\ L\odot$ to a minimum of $L_n \sim 29650\ L\odot$, a reduction of over 30 per cent. At minimum L_n, gravitational energy is released at the rate $L_g \sim 17780\ L\odot$, or at 60 per cent of the nuclear-energy production rate. On the other hand, during the gravitational contraction phase in the 9 $M\odot$ star, the rate of

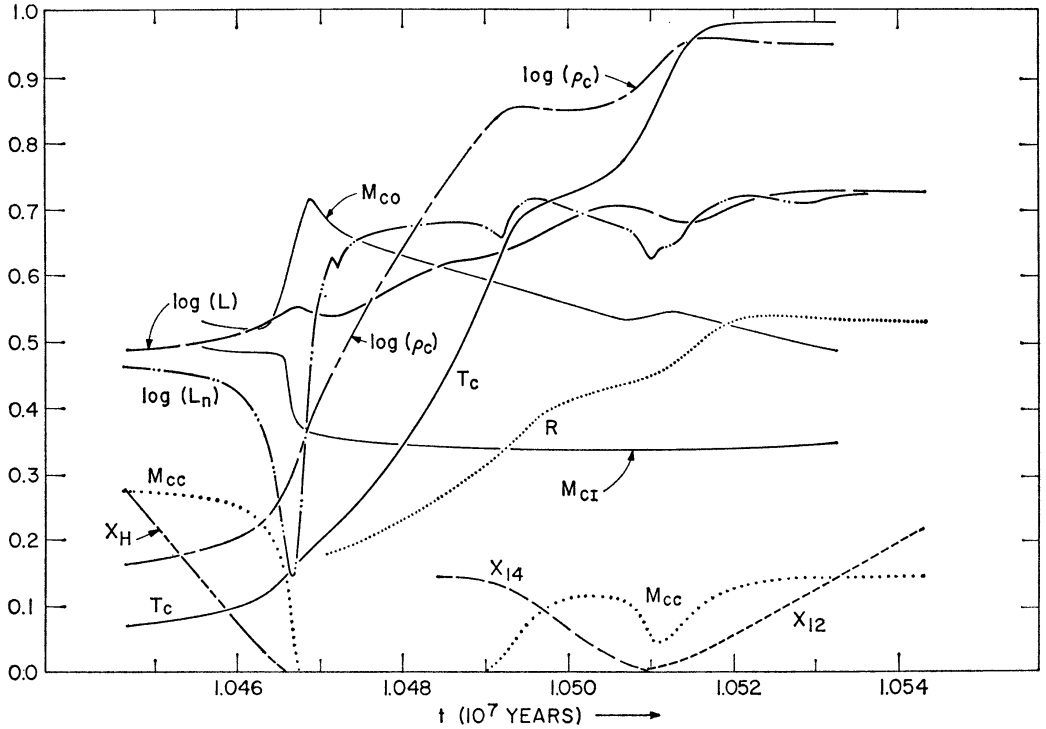

FIG. 4.—The variation with time t (units of 10^7 yr.) of central density (ρ_c), central temperature (T_c), luminosity (L), rate of nuclear-energy production (L_n), stellar radius (R), mass fraction of the inner and outer boundaries of the major convective layer (M_{CI} and M_{CO}), and the central abundances by mass of $H^1(X_H)$, $N^{14}(X_{14})$, and $C^{12}(X_{12})$. Units for T_c, ρ_c, L, and R are the same as in Figs. 2 and 3. L_n has the same units as L. Scale limits correspond to $4.4 \leq \log (L), \log (L_n) \leq 4.9$, $40 \leq T_c \leq 165$, $0.75 \leq \log (\rho_c) \leq 3.25$, $0 \leq R \leq 50$, $0 \leq M_{cc}, M_{CI}, M_{CO} \leq (\frac{2}{3})$, $0.0 \leq X_H \leq 0.01$, $0.0 \leq X_{12}, X_{14} \leq 0.10$.

nuclear-energy production drops by only 6 per cent and, at minimum L_n, gravitational energy is released at a rate which is only 16 per cent of the nuclear-energy production rate.

Toward the end of the over-all contraction phase and during the first portion of the phase of hydrogen-shell development, the innermost of the two convective layers grows rapidly in the 15 $M\odot$ star. The inner and outer boundaries of this layer are defined by the curves M_{CI} and M_{CO} in Figure 4. Just as in the 9 $M\odot$ star, this growth is a consequence of an increased energy flux engendered not only by the increase in interior luminosities, but also by the decrease in the cross-sectional area through which energy flows. After the development of the shell, the convective layers decrease gradually in size, finally disappearing when $t \cong 1.10 \times 10^7$ yr.

Conditions in the star at $t = 1.04693 \times 10^7$ yr, when the major convective layer has just passed its maximum size, are shown in Figures 5 and 6. The major convective layer

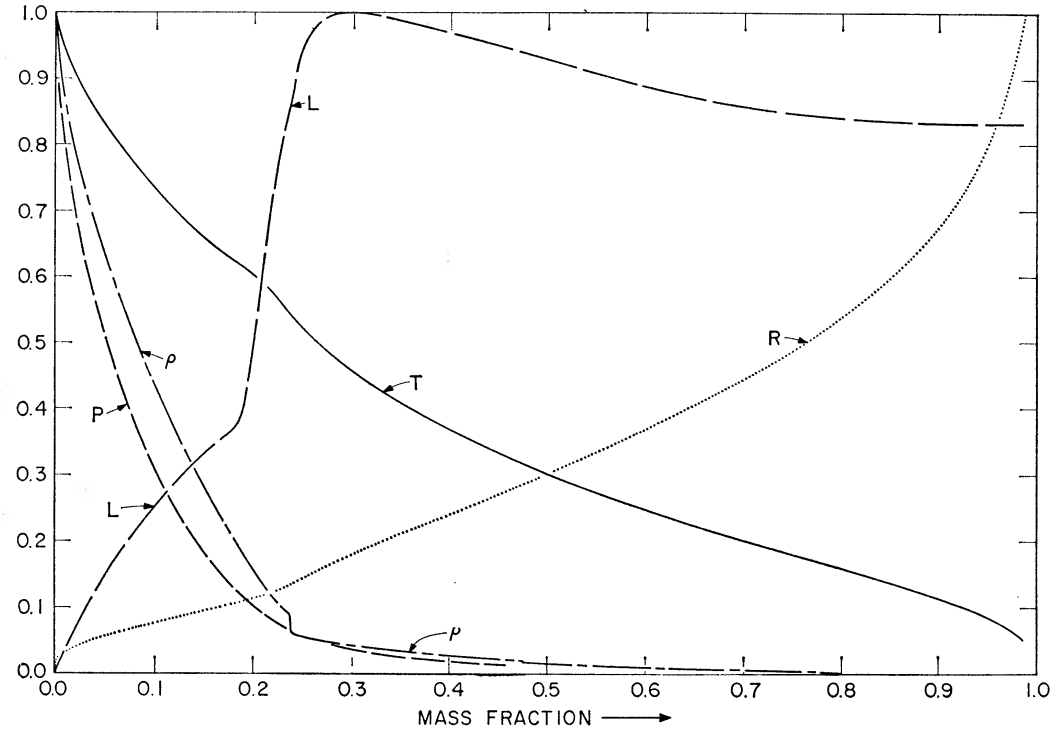

FIG. 5.—The variation with mass fraction of state variables when $t = 1.04693 \times 10^7$ yr. Variables have the significance (and physical units): P = pressure (10^{17} dynes/cm^2), T = temperature (10^6° K), ρ = density (gm/cm^3), L = luminosity (3.86×10^{33} ergs/sec), and R = radius (6.69×10^{10} cm). Scale limits correspond to $0.0 \leq P \leq 2.47603$, $0.0 \leq T \leq 63.6549$, $0.0 \leq \rho \leq 52.5432$, $0.0 \leq L \leq 56865.6$, and $0.0 \leq R \leq 5.34827$. The mass fraction in the static envelope is 0.0128903 and the stellar radius is $R_s = 8.66432\, R_\odot$.

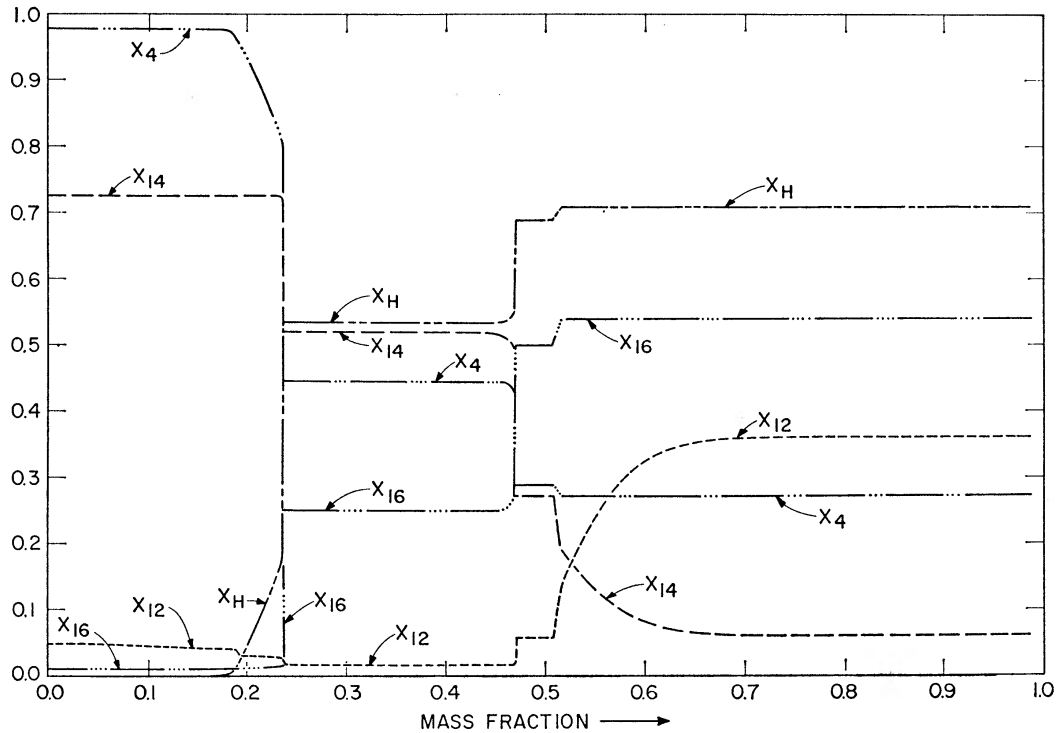

FIG. 6.—The variation with mass fraction of composition variables when $t = 1.04693 \times 10^7$ yr. The X_i are abundances by mass of H^1(X_H), He^4(X_4), C^{12}(X_{12}), N^{14}(X_{14}), and O^{16}(X_{16}). Scale limits correspond to $0.0 \leq X_H, X_4 \leq 1.0$, $0.0 \leq X_{12} \leq 0.01$, and $0.0 \leq X_{14}, X_{16} \leq 0.02$.

is located between mass fractions 0.4767 and 0.5060. Nuclear energy is produced in the hydrogen-burning shell at the rate $L_H \sim 51817\ L_\odot$, and gravitational energy is released in the hydrogen-exhausted core (between the stellar center and mass fraction $\sim$0.17) at the rate $(L_g)_{core} \sim 21300\ L_\odot$. Absorption between the shell center and the stellar surface occurs at the approximate rate of $L_{abs} \sim 16250\ L_\odot$. Expansion and cooling occur beyond mass fraction 0.449; contraction and heating prevail interior to this mass fraction. The division between outward and inward mass motions coincides very nearly with the division between contraction and expansion.

It was found in previous papers that, during the shell-development stage and the period of thick-shell hydrogen burning, the relative extent and duration of central cooling diminish with increasing stellar mass. In the 15 $M_\odot$ star, central cooling does not occur and the gravitational energy released by the contracting core continues to maintain a relatively steep gradient between the stellar center and the base of the shell.

Core temperatures continue to rise during and after shell development, reaching high enough values to fire the $N^{14}(\alpha,\gamma)F^{18}(\beta^+\nu)O^{18}$ reactions before the shell begins to narrow appreciably in mass fraction. Energy produced by the $N^{14} \rightarrow O^{18}$ conversion forces the development of a convective core (see curves X_{14} and M_{cc} in Fig. 4). As central N^{14} is reduced to nominal values, the convective core begins to recede, but energy generation by the triple-α process forces it to increase again in mass fraction (see curves X_{12} and M_{cc} in Fig. 4). The stellar radius decreases for a period of $\sim 2 \times 10^4$ yr (see the curve R versus t in Fig. 4 and the evolutionary path near point 7 in Fig. 1) and then increases gradually as the star enters the major phase of core helium burning.

IV. THE CORE HELIUM-BURNING PHASE

Contrary to its behavior in less massive stars, which reach the region of red giants and develop a deep convective envelope before embarking on the helium-burning phase, the radius of the 15 $M_\odot$ star continues to increase throughout most of the period of core helium burning (see R versus t in Fig. 3). Shortly after the beginning of the triple-α process in the core ($t \sim 1.0601 \times 10^7$ yr) and continuing throughout the period of increasing stellar luminosity, the rate of energy production in the hydrogen-burning shell decreases monotonically (see L_H in Fig. 3 and log (L) in Fig. 2). This is exactly the reverse of what occurs in lighter stars.

That envelope contraction and an increase in shell strength should occur together in the lighter stars, while envelope expansion and a decrease in shell strength should occur together in the more massive star, might not have been anticipated a priori. That the opposite behavior occurs in the two classes of stars is presumably a consequence of differences in envelope opacity and in the quite different relationship between core structure and envelope structure at the initiation of the triple-α process.

Prior to and during core helium burning, the opacity source throughout the 15 $M_\odot$ star is almost entirely temperature- and density-independent electron scattering. Energy transfer through the envelope is solely by radiative diffusion. In the lighter stars, prior to the major helium-burning phase, convection transports energy over a major fraction of the matter between the shell and the surface. In envelope regions not unstable against convection, energy transfer by radiative diffusion is controlled by a density- and temperature-dependent opacity.

The 15 $M_\odot$ star spends almost 90 per cent of the core helium-burning phase in the region between points 7 and 10 in Figure 1. Conditions in the stellar interior at $t = 1.135396 \times 10^7$ yr, approximately halfway between points 8 and 9, are shown in Figure 7. Energy production in the core, where $X_4 = 0.458$, $X_{12} = 0.236$, and $X_{16} = 0.276$, contributes 33 per cent of the total nuclear energy produced per second. Absorption in the expanding envelope is negligible. The redistribution of hydrogen and helium brought about by layer convection after the main-sequence phase is still very much in evidence.

After reaching point 10 in Figure 1, the rate at which the 15 $M_\odot$ star passes through

the H-R diagram begins to accelerate. Passage through the observational Cepheid strip (taken as a linear extension of the strip defined in Fig. 1 of Paper III), between log (T_e) = 3.679 and log (T_e) = 3.659, requires only 865 yr. Shortly after passing through the Cepheid strip, envelope convection assumes a dominant importance and the star begins to ascend steeply in the H-R diagram. Passage up the giant branch will be halted only when central temperatures reach high enough values to ignite the next nuclear fuel. In the present instance ($\sigma_{412} = \sigma^0_{412}$) this fuel will be O^{16}.

Conditions within the star at $t = 1.211213 \times 10^7$ yr, near the end of the evolutionary path in Figure 1 (log (T_e) = 3.6103, log (L) = 4.8418), are shown in Figure 8. Central

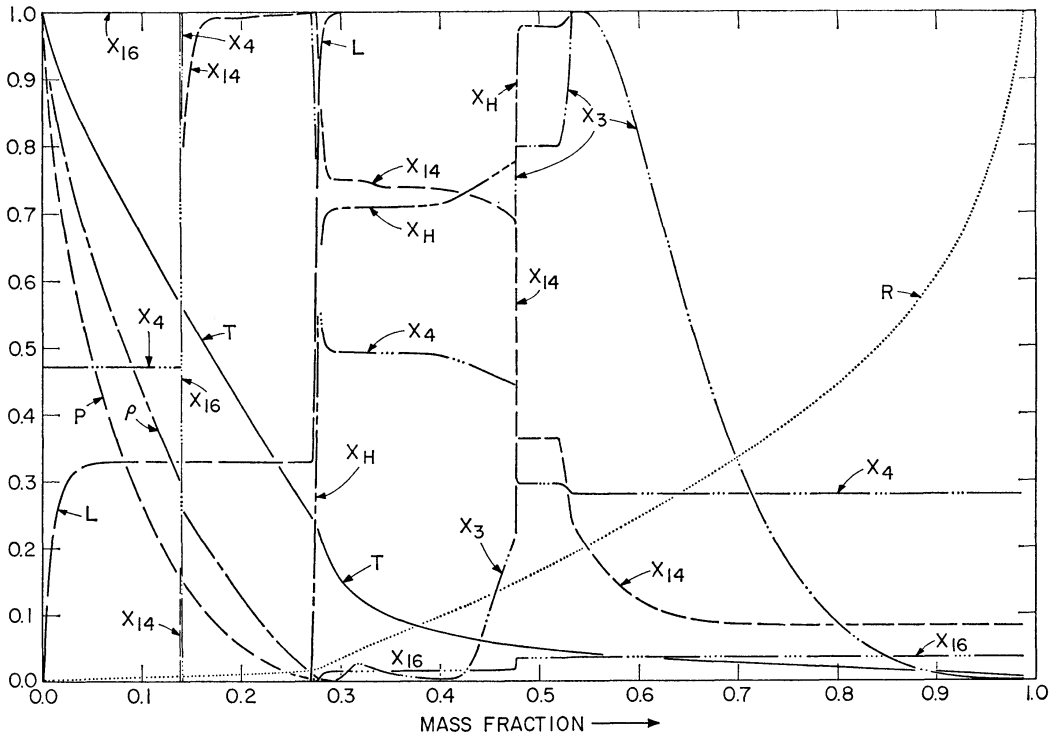

FIG. 7.—The variation with mass fraction of state and composition variables when $t = 1.13540 \times 10^7$ yr. Variables have the same significance and units as in Figs. 5 and 6. The abundance by mass of He^3 is given by X_3. Scale limits correspond to $0.0 \leq P \leq 139.542$, $0.0 \leq T \leq 179.734$, $0.0 \leq \rho \leq 1163.58$, $0.0 \leq L \leq 67890.7$, $0.0 \leq R \leq 20.4101$, $0.0 \leq X_H \leq 0.708$, $0.0 \leq X_3 \leq 1.740 \times 10^{-5}$, $0.0 \leq X_4 \leq 0.9761$, and $0.0 \leq X_{14} \leq 1.452 \times 10^{-2}$. The mass fraction in the static envelope is 0.0128903 and the stellar radius is $R_s = 38.0497\ R_\odot$.

abundances include $X_4 = 0.0123$, $X_{12} = 1.38 \times 10^{-3}$, $X_{16} = 0.955$, and $X_{22} = 2.28 \times 10^{-2}$. The rate at which gravitational energy is released at the center is about 2 per cent of the rate of nuclear-energy generation at the center. In the region between the center and the hydrogen-burning shell, gravitational energy is released at the rate of 9500 $L_\odot$.

Approximately one-half of the total rate of nuclear-energy production, $L_n = 68556\ L_\odot$, is contributed by the hydrogen-burning shell. The remainder is contributed by helium burning in the convective core (mass fraction $M_{cc} = 0.16575$) and by the $N^{14} \rightarrow O^{18}$ reactions in a minor shell centered at mass fraction $\sim$0.227. Absorption in the expanding envelope reduces the rate at which energy reaches the surface by $L_{abs} \sim 8593\ L_\odot$.

As may be seen from the distribution of He^3 in Figure 8, the mass fraction in the

convective envelope at $t = 1.211213 \times 10^7$ yr is $\Delta M_{CE} = 0.2013$. In the last model computed ($t = 1.211368 \times 10^7$ yr), the mass fraction in the convective envelope is $\Delta M_{CE} = 0.341$. Since central temperatures are rising at a rate of only $3.4 \times 10^7\,^\circ\mathrm{K}/10^4$ yr, whereas the mass fraction in the convective envelope is increasing at the rate of $0.905/10^4$ yr, it is probable that envelope convection will extend almost to the hydrogen-burning shell before the $2O^{16} \rightarrow S^{32}$ reactions begin in the core. On the basis of the abundance distributions in the last model computed, one may expect a considerable alteration in surface abundances when the star reaches the red-giant tip. Assuming that, at the red-giant tip, convection prevails over the outer 68.3 per cent of the star's mass, the surface

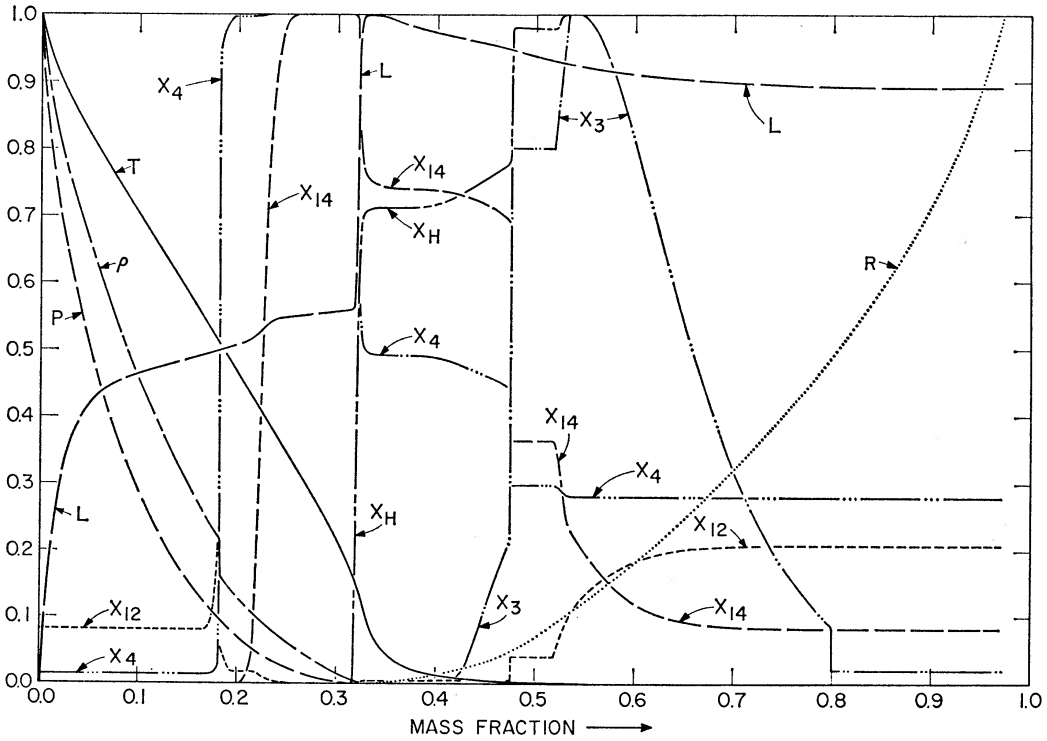

FIG. 8—The variation with mass fraction of state and composition variables when $t = 1.21121 \times 10^7$ yr. Variables have the same significance and units as in Figs. 5 and 6. Scale limits correspond to $0.0 \leq P \leq 727.258$, $0.0 \leq T \leq 294.552$, $0.0 \leq \rho \leq 3888.71$, $0.0 \leq L \leq 78115.7$, $0.0 \leq R \leq 414.339$, $0.0 \leq X_H \leq 0.7080$, $0.0 \leq X_3 \leq 1.740 \times 10^{-5}$, $0.0 \leq X_4 \leq 0.9760$, $0.0 \leq X_{12} \leq 1.744 \times 10^{-2}$, and $0.0 \leq X_{14} \leq 1.451 \times 10^{-2}$. The mass fraction in the static envelope is 0.0275827 and the stellar radius is $R_s = 530.383\ R_\odot$.

ratio of N^{14} to C^{12} will increase by a factor of 4.86 from an initial value of 0.333 to 1.62. The surface abundance of O^{16} will drop from 1.08×10^{-2} to 9.1×10^{-3}, the surface abundance of hydrogen will drop from 0.708 to 0.645, while the surface abundance of He^4 will increase from 0.272 to 0.335.

The conversion of O^{16} into Ne^{20} has not been included in the calculations. Using the maximum off-resonant rate for the $O^{16}(\alpha,\gamma)Ne^{20}$ reaction given by Fowler and Hoyle (1965), one finds that, at the center of the last model considered ($T_c = 299.57 \times 10^6\,^\circ\mathrm{K}$, $\rho_c = 4095.7$ gm/cm^3, $(X_{12})_c = 1.09 \times 10^{-3}$, $(X_{16})_c = 0.958$, $(X_4)_c = 0.0110$), only 1 α-particle is consumed by the $O^{16}(\alpha,\gamma)Ne^{20}$ reaction for every 28 which are consumed by the $C^{12}(\alpha,\gamma)O^{16}$ reaction. On the other hand, the conversion of Ne^{22} into Mg^{25} via the $Ne^{22}(\alpha,n)Mg^{25}$ reaction has probably proceeded to a considerable extent in the stellar core, thus providing neutrons for s-process synthesis. Because of the uncertainty in the cross-section, this reaction has not been explicitly considered.

Neutrino losses by the pair-annihilation process, though neglected in the present calculations, are of importance in the last models constructed. Using the loss rate by pair annihilation given by Fowler and Hoyle, neutrino losses at the center of the model described in Figure 8 ($T_c = 294.55 \times 10^6$ ° K, $\rho_c = 3888.7$ gm/cm^3) occur at the rate $\epsilon_{\nu\bar{\nu}} = -5.85 \times 10^4$ ergs gm^{-1} sec^{-1}. Nuclear and gravitational energy is released at the center at the rate $\epsilon_{\text{conventional}} = (\epsilon_{\text{nuc}} + \epsilon_{\text{grav}}) = 3.66 \times 10^5$ ergs gm^{-1} sec^{-1}, so that $(\epsilon_{\nu\bar{\nu}}/\epsilon_{\text{conventional}}) = -0.160$. At the center of the last model computed, the corresponding quantities are $\epsilon_{\nu\bar{\nu}} = -8.20 \times 10^4$ erg gm^{-1} sec^{-1} and $\epsilon_{\text{conventional}} = 3.24 \times 10^5$ ergs gm^{-1} sec^{-1}. Thus $(\epsilon_{\nu\bar{\nu}}/\epsilon_{\text{conventional}}) = -0.254$ and it is clear that neutrino losses will play an

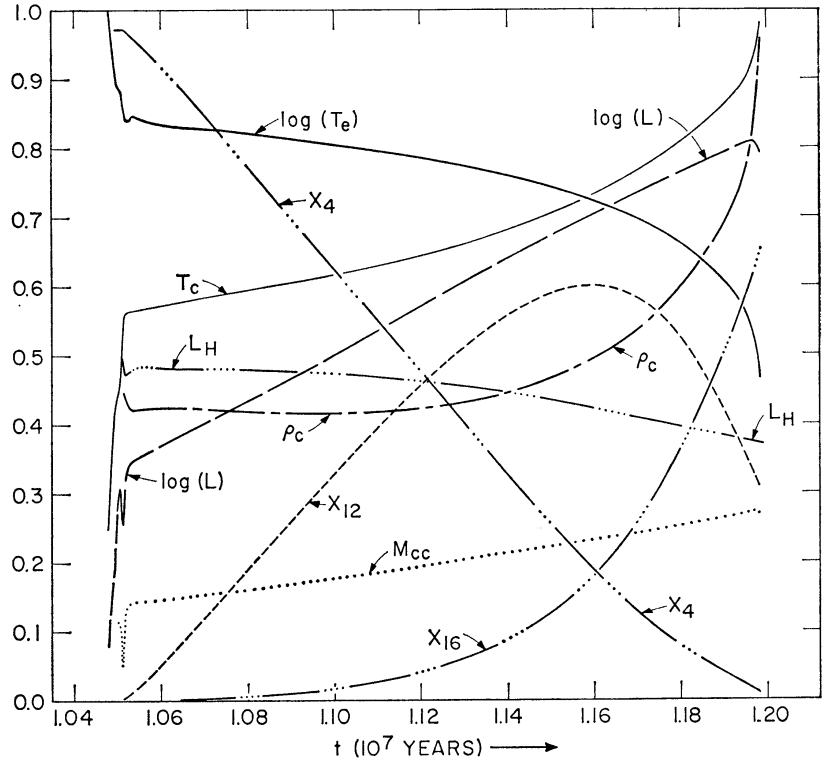

FIG. 9.—The variation with time t (units of 10^7 yr.) of several observable and interior characteristics when the cross-section for the $C^{12}(\alpha,\gamma)O^{16}$ reaction is chosen ten times smaller than that used in the main investigation. Variables have the same significance and physical units as in Figs. 2 and 3. Scale limits correspond to $4.675 \leq \log (L) \leq 4.925$, $3.4 \leq \log (T_e) \leq 4.4$, $20 \leq T_c \leq 270$, $500 \leq \rho_c \leq 3000$, $0 \leq M_{cc} \leq (\frac{2}{3})$, $0 \leq L_H \leq 10^5$, and $0.0 \leq X_4, X_{12}, X_{16} \leq 1.0$.

important role during the last stages of core helium burning as well as during subsequent evolutionary stages.

Hayashi and Cameron (1962*a*, *b*; 1964) have suggested that the distribution in the H-R diagram of stars in h and χ Persei (large population of red supergiants relative to the population of upper main-sequence stars and early giants) provides evidence against the occurrence of the photoneutrino and the pair-annihilation processes at the rate predicted by the conserved-vector-current theory of weak interactions.

The argument assumes that the evolution following the exhaustion of central helium will occur on a Kelvin-Helmholtz time scale and will not proceed again on a nuclear-burning time scale until central temperatures reach sufficiently high values for core carbon burning (if $\sigma_{412} < \sigma^0_{412}$) to reduce the rate of core contraction. Neutrino losses will presumably reduce the time scale for core nuclear burning by a considerable amount (relative to the time scale without neutrino losses) and reduce the time spent in the red-

giant region by a factor inconsistent with the large population of red supergiants in h and χ Persei. The validity of this argument rests on the assumption that the massive red supergiants in h and χ Persei are in the core carbon-burning (or core oxygen-burning) phase.

It is suggested here that evolution along the red-giant branch, between the termination of core helium burning and the beginning of the next stage of core nuclear burning, may not be on a Kelvin-Helmholtz time scale. Neutrino losses from central regions may act as a refrigerant. That is, the energy necessary to supply neutrino losses may come in part from thermal motions, with the result that core temperatures will not increase as rapidly, relative to the increase in density, as would have been the case without neutrino losses. Thus, core neutrino losses may have the effect of prolonging the time spent along the red-giant branch during combined hydrogen- and helium-shell burning in the absence of a core source of nuclear energy.

V. THE EFFECT OF REDUCING THE $C^{12}(\alpha,\gamma)O^{16}$ CROSS-SECTION

A reduction by a factor of 10 in the $C^{12}(\alpha,\gamma)O^{16}$ center-of-mass cross-section has essentially no influence on the path of the 15 $M_\odot$ star in the H-R diagram during the core helium-burning phase (see Fig. 1). However, due to a decrease in the average energy released per α-particle consumed, the total time for the core helium-burning phase is slightly reduced from 1.571×10^6 yr to 1.442×10^6 yr.

The variation with time of pertinent observable and interior characteristics is shown in Figure 9. Except for the O^{16} and C^{12} abundances, all quantities in Figure 9 vary in a fashion so similar to the variations shown in Figures 2 and 3, that a discussion is unnecessary. From the point of view of its effect on more advanced evolutionary phases, the only change engendered by reducing the $C^{12}(\alpha,\gamma)O^{16}$ cross-section is an enhancement in the final core abundance of C^{12} relative to the final core abundance of O^{16} (see curves X_{12} versus t and X_{16} versus t in Figs. 2 and 9). Extrapolating to the time when $X_4 = 0$, final core abundances of C^{12} and O^{16}, in the case $\sigma_{412} = \sigma^0_{412}$, are found to be $X_{12} = 0.00$ and $X_{16} = 0.966$. In the case $\sigma_{412} = \sigma^0_{412}/10$, final core abundances are $X_{12} = 0.294$ and $X_{16} = 0.672$.

Since, when $\sigma_{412} = \sigma^0_{412}$, the final result of helium burning in all stars with mass $M \geq 3M_\odot$ has been found to be O^{16}, the fact that C^{12} and O^{16} are of comparable abundance in the galactic disk suggests that the true cross-section for the $C^{12}(\alpha,\gamma)O^{16}$ reaction is perhaps closer to $\sigma^0_{412}/10$.

Special thanks are due to William A. Fowler for providing spiritual and material support. Thanks are due also to G. D. McCann for supplying time on the IBM 7094 at the California Institute of Technology in the spring and summer of 1964.

REFERENCES

Fowler, W. A., and Hoyle, F. 1964, *Ap. J. Suppl.*, No. 91.
Hayashi, C., and Cameron, R. C. 1962*a*, *Ap. J.*, **136**, 166.
———. 1962*b*, *A.J.*, **67**, 577.
———. 1964, *ibid.*, **69**, 140.
Iben, Icko, Jr. 1965*a*, *Ap. J.*, **141**, 993 (Paper I).
———. 1965*b*, *ibid.*, **142**, 1447 (Paper II).
———. 1966*a*, *ibid.*, **143**, 483 (Paper III).
———. 1966*b*, *ibid.*, p. 505 (Paper IV).
Sakashita, S., and Hayashi, C. 1961, *Prog. Theoret. Phys.* (Kyoto), **26**, 942.
Sakashita, S., Ono, Y., and Hayashi, C. 1959, *Prog. Theoret. Phys.* (Kyoto), **21**, 315.
Schwarzschild, M., and Härm, R. 1958, *Ap. J.*, **128**, 348.
Stothers, R. 1963, *Ap. J.*, **138**, 1074.